THE TEMPERATURE AND WAVELENGTH DEPENDENCE OF THE PHOTO-OXIDATION OF PROPIONALDEHYDE

JULIAN HEICKLEN, JAYANT DESAI, ABRAHA BAHTA, CHARLES HARPER and R. SIMONAITIS

Department of Chemistry and Communications and Space Sciences Laboratory, The Pennsylvania State University, University Park, PA 16802 (U.S.A.)

(Received November 21, 1985; in revised form February 13, 1986)

Summary

Propionaldehyde was photolyzed by flash photolysis in the presence of air or by steady state photolysis in the presence of O_2 at 298 or 263 K. For the flash photolysis experiments, the transient absorption of RO_2 radicals was monitored and quantum yields were obtained at 293.7, 302.0, 311.7 and 325.0 nm incident radiation. For the steady state photolysis, quantum yields for both CO and C_2H_6 were monitored at 253.7, 312.8 and 334.1 nm incident radiation. C_2H_6 was found at 253.7 nm but not at the longer wavelengths. For the steady state photolysis, the difference between the quantum yields for CO and C_2H_6 corresponds to the quantum yield of C_2H_5 formation. Good agreement was obtained for the radical yields by both methods. The radical yields decreased with increasing pressure, increasing wavelength or decreasing temperature. At 298 K, the half-quenching pressures were ∞, 7800 Torr, 5100 Torr, about 750 Torr, 308 Torr and 291 Torr at 254 nm, 294 nm, 302 nm, 312 nm, 325 nm and 334 nm respectively. These lead to atmospheric photodissociation coefficients for radical formation at 298 K of 2.4×10^{-5} s^{-1} and 1.6×10^{-5} s^{-1} for solar zenith angles of 30° and 58° respectively.

1. Introduction

The photo-oxidation of the low molecular weight aliphatic aldehydes is an important source of free-radical production in the polluted urban atmosphere [1]. These radical products are responsible for driving the chemical cycles which convert NO to NO_2. Therefore knowledge of the radical yields from aldehyde photo-oxidation is essential for the purposes of tropospheric modelling. The simple aliphatic aldehydes studied include CH_2O [2 - 24], CH_3CHO [2, 24 - 43] and C_2H_5CHO [44 - 51].

For C_2H_5CHO there are three possible primary photodecomposition paths:

0047-2670/86/$3.50

$$P + h\nu \longrightarrow C_2H_6 + CO \quad (1a)$$

$$\longrightarrow C_2H_5 + HCO \quad (1b)$$

$$\longrightarrow C_2H_5CO + H \quad (1c)$$

where P stands for C_2H_5CHO.

In the presence of O_2, both HCO and H quantitatively give HO_2:

$$HCO + O_2 \longrightarrow HO_2 + CO \quad (2)$$

$$H + O_2 + M \longrightarrow HO_2 + M \quad (3)$$

Blacet and Pitts [44] have studied the photolysis of C_2H_5CHO in the wavelength region 238 - 334 nm. They found that process (1a) increased and process (1b) decreased in importance as the wavelength was decreased. However, the sum of the measured primary process quantum yields did not equal unity, presumably due to some excited state quenching by added I_2. Hansen and Lee [49] have found that the fluorescence quantum yield is unimportant over most of this wavelength range. Shepson and Heicklen [50] found that at 313 nm ϕ_{1b} is unity at low pressures; but the excited state precursor to radical formation is pressure quenched. In air, both primary processes (1a) and (1b) lead to the production of CO, and process (1a) also leads to the production of C_2H_6. Thus $\Phi(C_2H_6)$ is a measure of primary process (1a) and $\Phi(CO) - \Phi(C_2H_6)$ is a measure of primary process (1b). The CO quantum yield decreases with increasing pressure of air from a value of unity at low pressures [51]. Shepson and Heicklen [51] also found that the Stern–Volmer plots of ϕ_{1b}^{-1} *versus* [M] are linear at four wavelengths (326, 302, 280 and 254 nm) but show marked deviation from linearity at 334 and 313 nm. The CO must come from some precursor which can be removed by collision. This precursor is believed to be the vibrationally excited triplet state ^3P_n, so that the competing processes are

$$^3P_n \longrightarrow C_2H_5 + HCO \quad (4)$$

$$^3P_n + M \longrightarrow \text{quenching} \quad (5)$$

Values of k_4/k_5 at the various wavelengths are summarized in Table 1. For the static steady state photolysis experiments in which the Stern–Volmer quenching plot was not linear, two values of k_4/k_5 are reported, assuming two quenching processes. To investigate these findings further, we have undertaken a study of the laser flash photolysis of C_2H_5CHO in the presence of O_2 or air and measured $C_2H_5O_2$ radical yields, the $C_2H_5O_2$ coming from

$$C_2H_5 + O_2 \longrightarrow C_2H_5O_2 \quad (6)$$

This method should provide a direct measure for primary process (1b). We have also reinvestigated the steady state photolysis of C_2H_5CHO in O_2 to check the earlier studies and extend them to lower temperatures.

TABLE 1

Half-quenching pressure (k_4/k_5) in the photo-oxidation of C_2H_5CHO[a]

λ (nm)	*Temperature* (K)	k_4/k_5 (Torr)			
		Shepson and Heicklen [50]	*Shepson and Heicklen* [51]	*This work, steady state photolysis*	*This work, flash photolysis*
254	298		280	∞[b]	
254	263			∞[b]	
280	298		610		
294	298				7800 ± 4800
302	298		225		5100 ± 2700
302	263				1448 ± 192
312	298	630, 70[c]	570, ≈45[c]	699 ± 41	798 ± 102
312	263			390 ± 21	
325	298		57		308 ± 38
334	298		325, ≈24[c]	291 ± 25	

[a]Uncertainties are one standard deviation.
[b]Too large to measure.
[c]Non-linear Stern–Volmer quenching plot. Two half-quenching pressures are reported, assuming two quenching processes.

2. Experimental details

2.1. Flash photolysis

C_2H_5CHO (13 - 30 Torr) was photolyzed with a frequency-doubled Phase-R DL 1100 dye laser at 293.7, 302.0, 311.7 and 325.0 nm (uncertainty in wavelength measurement, ±0.3 nm) in the presence of 30 - 650 Torr of dry room air. The arrangement of the apparatus is essentially as described before [42]. All gases were handled in a conventional glass vacuum line containing Teflon stopcocks with Viton O-rings. The Cl_2 pressure was measured using an H_2SO_4 manometer, the C_2H_5CHO pressure using a Wallace and Tiernan model FA-160 0 - 50 Torr absolute pressure indicator and the air using a calibrated NRC 820 Alphatron gauge.

The low temperature Pyrex reaction cell was 45.2 cm long and 2.7 cm in diameter. At each end were quartz windows. The cell was encased in two jackets. Liquid ethanol was cooled to 263 ± 1 K with dry ice and circulated through the inner jacket. The ethanol was circulated using a Neslab Instrument Inc. Cryoflow A fluid circulating pump (Model 10389) and reservoir "U-tainer A". The outer jacket was evacuated to provide insulation. The temperature was monitored using a thermocouple or a precision thermometer.

Actinometry for quantum yield determination was done by photolyzing optically equivalent Cl_2–O_2–C_2H_6 mixtures (4 - 8 Torr Cl_2 in 45 Torr O_2 which contained about 5.5 mol.% hydrocarbon). The absorption cross sections used for both C_2H_5CHO and Cl_2 were measured in our laboratory. Table 2 lists our values of these absorption cross sections together with those from the literature. The photolysis of the Cl_2–O_2–C_2H_6 mixture provides the $C_2H_5O_2$ radical with a quantum yield of 2.0. The quantum yield in an experimental run is computed as twice the relative intensity of the signal in experimental and actinometer runs divided by the corresponding relative energy input at matched absorbances of CH_3CHO and Cl_2 respectively.

TABLE 2

Absorption cross sections σ for C_2H_5CHO and Cl_2 at 25 °C

λ (nm)	$10^{20}\sigma$ [a] (cm^2)	$10^{20}\sigma$ [b] (cm^2)
C_2H_5CHO		
293.7	4.72	5.10
302.0	5.00	4.91
311.7	3.44	3.38
325.0	1.00	1.07
Cl_2		
293.7	7.90	8.15
302.0	12.9	13.1
311.7	17.0	19.4
325.0	25.0	25.1

[a] This work; band halfwidth, 8 nm.
[b] Values for C_2H_5CHO, from Calvert and Pitts [52]; for Cl_2, from NASA [53].

2.2. Steady state photolysis

The steady state photolysis at room temperature was performed in three cylindrical Pyrex cells fitted with quartz windows. One cell was 770 ml with windows 7.0 cm in diameter, the second cell was 1270 ml with windows 9.0 cm in diameter and the third cell was 463 ml with windows 5.0 cm in diameter. The total pressure was brought to the desired value by adding dry O_2. The gases were introduced into the reaction cell from a conventional grease-free vacuum line with Teflon stopcocks. The reactions at low temperature were performed in another cylindrical reaction cell which was 22 cm long and 5 cm in diameter, fitted with quartz windows on both ends. Ethanol, which was cooled by dry ice, was circulated through an outer jacket by another Neslab cooling system (described above) to cool the reaction mixture. The reaction mixture and the cooling jacket were enclosed by a coaxial cylindrical jacket which was evacuated to insulate the cell. The entire cell was enclosed in a light-tight wooden box. The temperature was monitored using a mercury thermometer and could be maintained to ±3 K.

The experiments were performed at wavelengths of 253.7, 312.8 and 334.1 nm. A Hanovia medium pressure lamp (type SH) together with a Hanovia lamp stabilizer (type 30620) was used for the 312.8 and 334.1 nm lines. The 312.8 and 334.1 nm lines were isolated by using Corion SM 3130-2 and SM 3340-2 interference filters respectively. The bandwidth (full width at half-maximum) of these filters is approximately 8 nm. For the experiments at 253.7 nm a low pressure U-shaped mercury lamp from Conrad Hanovia (model 687-A45) was used. The 184.9 nm line was removed by absorption in air before striking the cell.

CO and C_2H_6 were the products of interest and were determined by gas chromatography using a Gow-Mac model 40-05D gas chromatograph with a thermal conductivity detector. CO was separated on a stainless steel column (5 ft × 1/4 in) packed with 5A molecular sieve. C_2H_6 was separated on a Teflon column (10 ft × 1/4 in) packed with Chromosorb 101 (diatomaceous earth). The molecular sieve column was operated at room temperature with a helium flow rate of 60 ml min^{-1} whereas the Chromosorb 101 column was operated at 363 K with a helium flow rate of 40 ml min^{-1}.

Azomethane was used as an actinometer for the wavelengths 312.8 and 334.1 nm. The N_2, which is produced with a quantum yield of 1.0 [52], was determined by gas chromatography using a stainless steel column (5 ft × 1/4 in) packed with 5A molecular sieve.

Phosgene ($COCl_2$) was used as an actinometer for the experiments performed at 253.7 nm. $COCl_2$ gives CO with a quantum yield of 1.0 [54]. The CO produced was determined as described earlier.

2.3. Materials and their purification

C_2H_5CHO (Aldrich, 99+%) was degassed at 77 K and used without further purification. Cl_2 (Matheson, research grade) was passed over KOH to remove HCl and degassed at 77 K. The Matheson O_2, CO and C_2H_6 used

were extra dry, chemically pure and research grade respectively. Laboratory air was used after being dried by rapid passage through a trap at 77 K.

The azomethane was prepared from dimethylhydrazine and HgO using a modified procedure reported by Renaud and Leitch [55]. It was purified by trap-to-trap distillation from 183 to 142 K. The $COCl_2$ was chemically pure grade from Air Products and was distilled from 183 to 146 K before use.

3. Results

3.1. Flash photolysis

When C_2H_5CHO–O_2 or Cl_2–O_2–C_2H_6 mixtures are flash photolyzed with the laser, a transient absorption is seen at 250 nm. A sample absorption trace is shown in Fig. 1. After the flash, the absorption remains constant for more than 100 μs. If this absorption is attributed solely to $C_2H_5O_2$, then the quantum yields Φ(rad) of $C_2H_5O_2$ can be computed. These values are listed in Table 3 as a function of air pressure and incident wavelength. At low pressure the quantum yields are approximately unity for each wavelength studied. However, as is evident from Table 3, as the air pressure is increased, a decrease in quantum yield is observed at 311.7 and 325.0 nm.

In practice the absorption observed is not due solely to $C_2H_5O_2$. If process (1c) occurs, then $C_2H_5C(O)O_2$ will also be present. Also there is one HO_2 formed for each $C_2H_5O_2$ and for each $C_2H_5C(O)O_2$. Thus

$$\Phi(\text{rad}) = (1 + \beta_1)\Phi(C_2H_5O_2) + (\beta_1 + \beta_2)\Phi(C_2H_5C(O)O_2) \quad \text{(I)}$$

where

$$\beta_1 = \frac{\sigma(HO_2)}{\sigma(C_2H_5O_2)}$$

$$\beta_2 = \frac{\sigma(C_2H_5C(O)O_2)}{\sigma(C_2H_5O_2)}$$

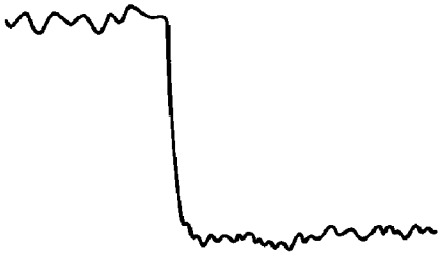

Fig. 1. Plot of light intensity at 250 nm *vs.* time after the flash in the 302.5 nm photolysis of a mixture of C_2H_5CHO at 15.0 Torr and air at 303.3 Torr. The time scale runs from left to right with a sweep time of 2 μs per channel. The total time of the trace is about 500 μs. The fraction of light absorbed is 0.012. The plot is an average of eight shots.

TABLE 3

Quantum yields of radical formation for the flash photolysis of C_2H_5CHO in air

Total pressure (Torr)	E[a]	N[b]	Φ(rad)
λ = 293.7 ± 0.3 nm, T = 298 ± 2 K, [C_2H_5CHO] = 14.2 ± 0.9 Torr			
36.8	0.465	4	0.97
36.8	0.517	16	0.93
36.8	0.501	16	0.99
38.6	0.260	8	1.19
38.6	0.245	16	0.98
38.6	0.216	32	1.24
40.0	0.386	4	1.10
40.0	0.384	8	1.10
40.0	0.302	16	1.20
65.3	0.436	8	0.96
65.3	0.439	16	1.02
65.3	0.423	16	0.96
91.7	0.209	16	1.08
91.7	0.173	16	0.99
92.4	0.338	8	1.20
92.4	0.329	16	1.13
278	0.311	8	1.22
278	0.293	32	0.93
626	0.414	32	0.99
626	0.389	32	0.85
683	0.370	32	0.91
683	0.310	32	1.09
692	0.285	32	1.06
692	0.274	32	0.98
692	0.243	32	1.00
λ = 302.0 ± 0.3 nm, T = 298 ± 2 K, [C_2H_5CHO] = 15.4 ± 2.8 Torr			
40.4	0.182	32	1.14
43.6	0.144	32	1.06
44.6	0.189	8	1.04
44.6	0.168	8	1.09
44.6	0.318	32	1.18
45.3	0.236	8	0.98
45.3	0.226	8	1.03
45.3	0.200	32	1.14
95.2	0.213	32	1.03
99.4	0.110	32	0.89
104	0.253	8	0.90
104	0.218	8	1.01
105	0.176	32	1.11
111	0.318	32	1.09
179	0.162	32	1.15
241	0.184	32	0.85
243	0.208	8	0.91
243	0.180	8	0.94
264	0.295	32	0.99
299	0.163	8	0.96

(continued)

TABLE 3 *(continued)*

Total pressure (Torr)	E [a]	N [b]	Φ(rad)
299	0.152	8	0.96
452	0.136	64	1.00
482	0.173	64	1.08
535	0.167	16	0.88
535	0.166	16	0.89
570	0.255	32	1.16
653	0.165	16	0.90
λ = 302.0 ± 0.3 nm, T = 263 ± 1 K, [C_2H_5CHO] = 15.0 ± 1.0 Torr			
43.8	0.193	16	1.10
43.8	0.187	16	1.10
44.1	0.240	16	1.19
44.1	0.255	16	1.16
44.9	0.141	16	1.12
44.9	0.152	16	1.10
46.0	0.291	16	1.17
46.0	0.209	16	1.19
99.4	0.147	16	1.08
104	0.175	16	1.12
107	0.228	16	1.14
112	0.244	16	1.16
189	0.148	16	1.06
271	0.249	16	0.98
271	0.185	16	1.15
285	0.249	16	1.10
500	0.252	16	0.83
500	0.221	32	0.89
646	0.184	16	0.97
646	0.160	32	0.96
646	0.151	16	0.82
646	0.152	16	0.76
660	0.242	16	0.76
660	0.224	16	0.74
λ = 311.7 ± 0.3 nm, T = 298 ± 2 K, [C_2H_5CHO] = 17.0 ± 1.2 Torr			
43.2	0.118	8	1.03
43.2	0.137	8	0.99
44.5	0.175	64	1.10
45.3	0.144	64	1.12
47.2	0.139	64	1.23
47.2	0.117	64	1.10
69.5	0.140	8	1.08
236	0.114	64	0.84
285	0.129	8	0.84
285	0.161	64	0.92
431	0.149	64	0.86
431	0.147	64	0.76
539	0.125	8	0.69
539	0.126	32	0.64

(continued)

TABLE 3 *(continued)*

Total pressure (Torr)	E [a]	N [b]	Φ(rad)
577	0.118	64	0.62
617	0.185	64	0.75
688	0.097	64	0.60
λ = 325.0 ± 0.3 nm, T = 298 ± 2 K, [C_2H_5CHO] = 19.7 ± 0.3 Torr			
46.1	0.188	32	1.15
46.1	0.155	32	1.20
46.4	0.239	32	0.99
46.4	0.317	32	1.12
48.0[c]	0.173	32	1.17
49.9	0.175	32	1.31
49.9	0.168	32	1.15
89.7[c]	0.166	32	1.07
111	0.163	32	1.06
111	0.161	32	1.07
202[c]	0.144	32	0.85
209	0.153	32	0.77
209	0.151	32	0.82
250	0.164	32	0.78
250	0.152	32	0.81
300[c]	0.159	32	0.72
348	0.246	32	0.78
348	0.229	32	0.77
375	0.167	32	0.53
375	0.161	32	0.54
598	0.228	32	0.44
598	0.211	32	0.48

[a] Average relative energy per shot.
[b] Number of laser shots.
[c] [C_2H_5CHO] = 25.5 Torr.

The extinction coefficients $\sigma(C_2H_5O_2)$ and $\sigma(HO_2)$ are 3.16×10^{-18} cm^2 and about 0.35×10^{-18} cm^2 respectively, at 250 nm [42]. Thus $\beta_1 \approx 0.11$. The value for β_2 is not known, but probably is about 1.0, since most RO_2 radicals are expected to have similar extinction coefficients.

Stern–Volmer plots of $\Phi(\text{rad})^{-1}$ *versus* the total pressure [M] are shown in Figs. 2 - 6. Actually, earlier results [50] suggested that C_2H_5CHO is 50% more efficient than air as a quencher. However, the quenching only occurs when air is in very large excess, so that neglecting the 50% correction on the C_2H_5CHO pressure is of no consequence. The plots are linear and give the intercepts α listed in Table 4. If $\beta_1 = 0.11$ and $\beta_2 = 1.0$, then the expected values for the intercepts are 0.90. The results are in reasonably good agreement with this expectation. The slopes γ of the respective plots are also listed in Table 4. The values of k_4/k_5 obtained from the ratio of the intercept to the slope are listed in Table 1.

TABLE 4

Evaluation of parameters[a]

λ (nm)	*Temperature* (K)	α^b	α^c	$10^3\gamma^b$ ($Torr^{-1}$)	$10^3\gamma^c$ ($Torr^{-1}$)
254	298	4.5 ± 0.2		0.0	
254	263	3.7 ± 0.3		0.0	
294	298		0.94 ± 0.03		0.12 ± 0.07
302	298		0.95 ± 0.03		0.19 ± 0.09
302	263		0.84 ± 0.02		0.58 ± 0.07
312	298	1.09 ± 0.02	0.86 ± 0.04	1.56 ± 0.07	1.08 ± 0.10
312	263	1.13 ± 0.03		2.90 ± 0.08	
325	298		0.73 ± 0.04		2.36 ± 0.17
334	298	1.97 ± 0.07		6.4 ± 0.3	

[a] $\Phi(rad)^{-1} = \alpha + \gamma[M]$, for laser flash photolysis; $\Phi(C_2H_5)^{-1} = \alpha + \gamma[M]$, for steady state photolysis.
[b] From steady state photolysis. Uncertainties are one standard deviation.
[c] From laser flash photolysis. Uncertainties are one standard deviation.

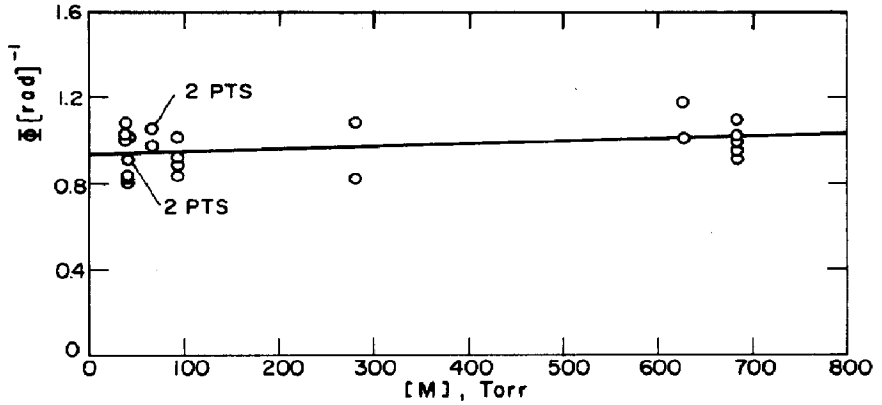

Fig. 2. Plot of $\Phi(rad)^{-1}$ *vs.* total pressure at 293.7 nm and 298 K from flash photolysis experiments.

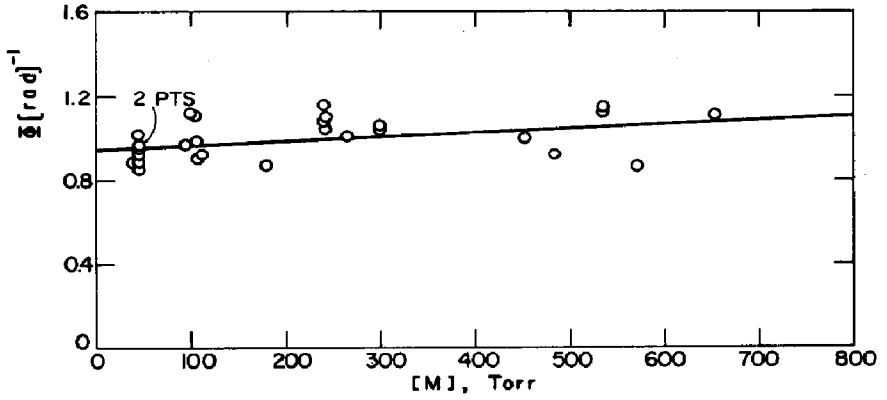

Fig. 3. Plot of $\Phi(rad)^{-1}$ *vs.* total pressure at 302.0 nm and 298 K from flash photolysis experiments.

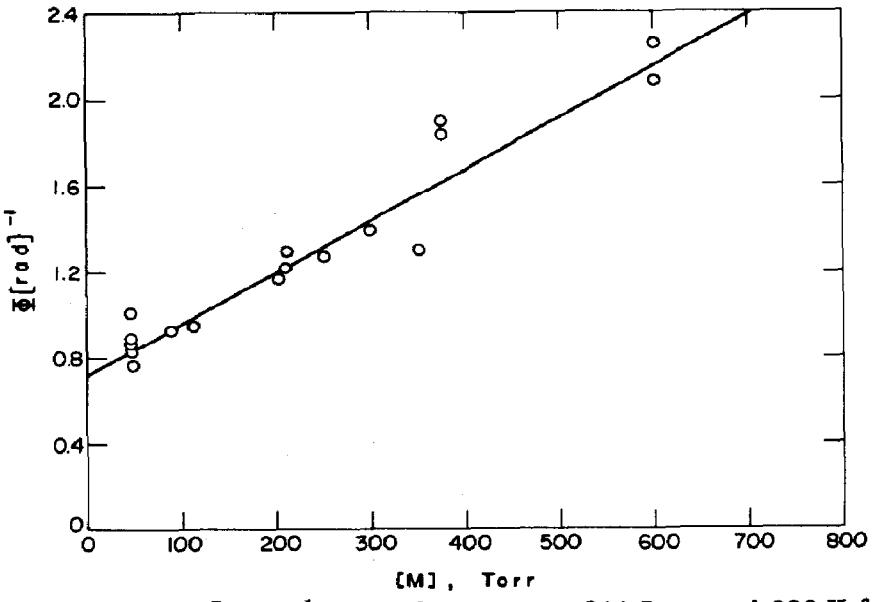

Fig. 4. Plot of $\Phi(\text{rad})^{-1}$ *vs.* total pressure at 311.7 nm and 298 K from flash photolysis experiments.

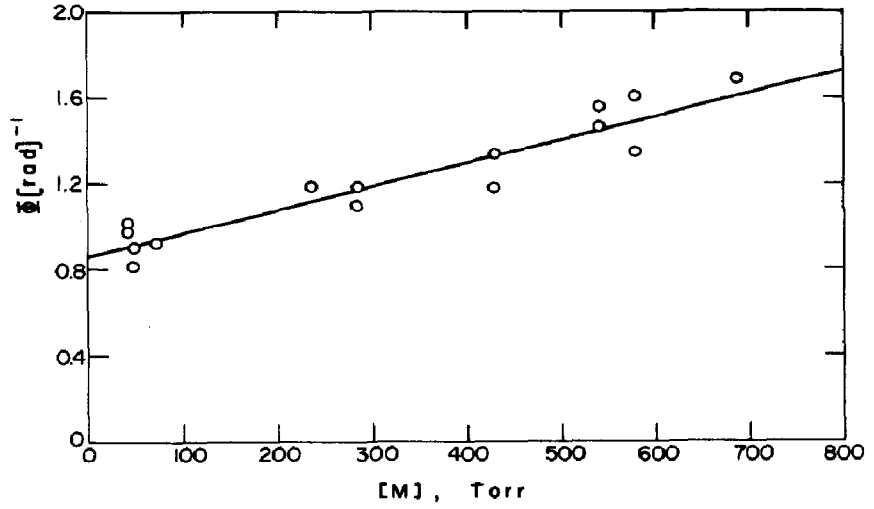

Fig. 5. Plot of $\Phi(\text{rad})^{-1}$ *vs.* total pressure at 325.0 nm and 298 K from flash photolysis experiments.

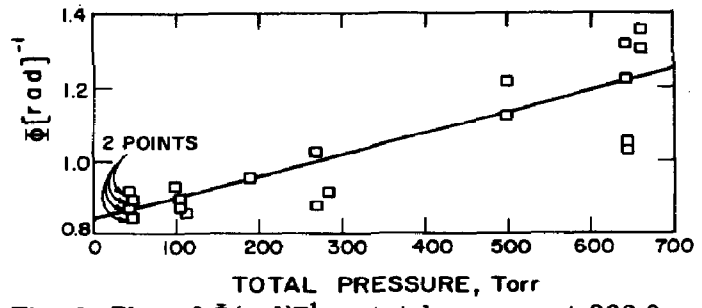

Fig. 6 Plot of $\Phi(\text{rad})^{-1}$ *vs.* total pressure at 302.0 nm and 263 K from flash photolysis experiments.

3.2. Steady state photolysis

C_2H_5CHO was photolyzed at several incident wavelengths in the presence of excess O_2. The products measured were CO and C_2H_6 since these products give a direct measure of the two photodecomposition pathways (1a) and (1b). C_2H_6 was found at 253.7 nm incident radiation, but not at the two longer wavelengths. The quantum yield $\Phi(C_2H_6)$ of C_2H_6 formation is a direct measure of the yield of the molecular process, whereas the quantum yield $\Phi(CO)$ of CO formation is a direct measure of the sum of the molecular and free radical processes. Thus the quantum yield $\Phi(C_2H_5)$ of reaction (1b) to form C_2H_5 radicals is given by $\Phi(CO) - \Phi(C_2H_6)$.

The effect of pressure on the quantum yields was measured at three incident wavelengths and two temperatures for $[C_2H_5CHO] = 10.1$ Torr. The results are shown for C_2H_6 formation in Table 5 and for CO formation in Table 6. For the C_2H_6 measurements, the extent of conversion was kept low to ensure that initial quantum yields were being measured. At all wavelengths both $\Phi(C_2H_6)$ and $\Phi(CO)$ fall with increasing pressure, though $\Phi(CO)$ and $\Phi(C_2H_6)$ at 253.7 nm reach lower limiting values.

As already stated, the ethyl-radical quantum yield $\Phi(C_2H_5)$ is given by

$$\Phi(C_2H_5) = \Phi(CO) - \Phi(C_2H_6) \qquad \text{(II)}$$

TABLE 5

Effect of total pressure on the C_2H_6 quantum yield for $[C_2H_5CHO] = 10.1 \pm 0.1$ Torr in steady state photolysis

Total pressure[a] (Torr)	*Irradiation time* (min)	$\Phi(C_2H_6)$
$\lambda = 253.7$ nm, $T = 298$ K, $I_a = 2.7 \times 10^{-4}$ photons min^{-1} per C_2H_5CHO molecule		
12.6	12.0	0.45
37	22.0	0.43
73	21.0	0.41
142	28.0	0.41
274	31.0	0.37
348	27.0	0.32
420	25.0	0.35
470	18.0	0.34
512	31.0	0.32
582	20.0	0.33
$\lambda = 253.7$ nm, $T = 263$ K, $I_a = 2.25 \times 10^{-4}$ photons min^{-1} per C_2H_5CHO molecule		
12.6	20.0	0.39
34	24.0	0.39
70	20.0	0.35
128	20.0	0.38
207	20.0	0.33
250	20.0	0.33
360	23.0	0.35
480	20.0	0.30

[a]Total pressure achieved by adding O_2.

The $\Phi(C_2H_5)$ are calculated using the experimentally measured values of $\Phi(CO)$ and $\Phi(C_2H_6)$ and are fitted to Stern–Volmer plots (Figs. 7 and 8):

$$\Phi(C_2H_5)^{-1} = \alpha + \gamma[M] \quad \text{(III)}$$

TABLE 6

Effect of total pressure on the CO quantum yield for $[C_2H_5CHO] = 10.1 \pm 0.1$ Torr in steady state photolysis

Total pressure[a] (Torr)	*Irradiation time* (min)	Φ(CO)
$\lambda = 253.7$ nm, $T = 298$ K, $I_a = 2.7 \times 10^{-4}$ photons min^{-1} per C_2H_5CHO molecule		
13.5	42.0	0.73
21	40.0	0.68
27	58.0	0.66
40	50.0	0.65
190	50.0	0.61
210	50.0	0.60
345	65.0	0.57
460	80.0	0.55
610	70.0	0.55
$\lambda = 253.7$ nm, $T = 263$ K, $I_a = 2.25 \times 10^{-4}$ photons min^{-1} per C_2H_5CHO molecule		
32	41.0	0.70
65	45.0	0.63
105	45.0	0.61
330	51.0	0.64
358	51.0	0.62
415	51.0	0.63
486	59.0	0.62
545	52.0	0.58
657	50.0	0.54
$\lambda = 312.8$ nm, $T = 298$ K, $I_a = 2.87 \times 10^{-4}$ photons min^{-1} per C_2H_5CHO molecule		
37	30.0	0.88
37	35.0	0.94
62	35.0	0.83
74	36.0	0.86
110	45.0	0.78
112	40.0	0.78
175	40.0	0.74
215	35.0	0.67
237	55.0	0.70
300	50.0	0.63
350	41.0	0.61
385	45.0	0.56
435	36.0	0.57
452	45.0	0.56
461	45.0	0.56
487	45.0	0.54
504	50.0	0.52
605	55.0	0.52

(continued)

TABLE 6 *(continued)*

Total pressure[a] (Torr)	*Irradiation time* (min)	Φ(CO)
λ = 312.8 nm, T = 263 K, I_a = 3.05 × 10^{-4} photons min^{-1} per C_2H_5CHO molecule		
31	45.0	0.80
72	37.0	0.75
75	35.0	0.74
170	37.0	0.59
277	45.0	0.52
365	56.0	0.46
387	50.0	0.44
450	60.0	0.42
475	50.0	0.41
560	65.0	0.37
720	85.0	0.30
λ = 334.1 nm, T = 298 K, I_a = 1.42 × 10^{-5} photons min^{-1} per C_2H_5CHO molecule		
18	730.0	0.54
25	725.0	0.52
52	780.0	0.43
95	840.0	0.38
175	1165.0	0.32
245	975.0	0.30
315	124.0	0.26
415	1445.0	0.22

[a]Total pressure achieved by adding O_2.

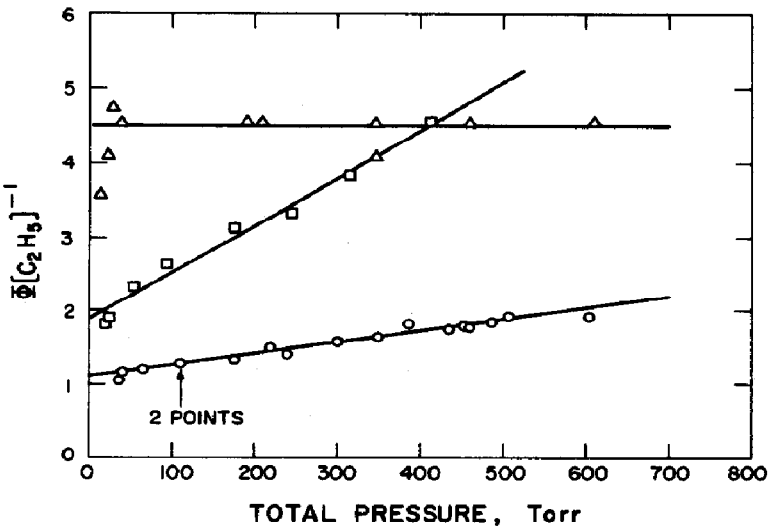

Fig. 7. Plots of $\Phi(C_2H_5)^{-1}$ *vs.* total pressure at 298 K from steady state photolysis: △, 253.7 nm; ○, 312.8 nm; □, 334.1 nm.

where α and γ are constants and $[M] = [O_2] + [C_2H_5CHO]$. The $\Phi(C_2H_5)^{-1}$ are plotted against total pressure at 298 K in Fig. 7 and at 263 K in Fig. 8. The plots are linear. The values of the intercepts α and the slopes γ are listed in Table 4. The ratios of the intercept to the slope give the half-quenching pressure k_4/k_5, and these are listed in Table 1; they decrease with decreasing temperature and increasing incident wavelength, *i.e.* they decrease with decreasing energy content of the initially formed excited state.

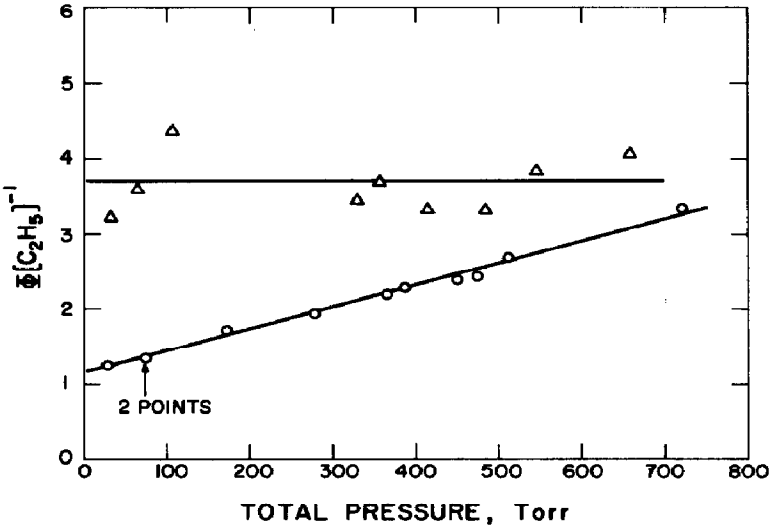

Fig. 8. Plots of $\phi(C_2H_5)^{-1}$ *vs.* total pressure at 263 K from steady state photolysis: △, 253.7 nm; ○, 312.8 nm.

4. Discussion

The results obtained for $\Phi(C_2H_6)$, *i.e.* the molecular process (1a), are similar to but slightly different from those obtained by Shepson and Heicklen [51] at 253.7 nm. Shepson and Heicklen found $\Phi(C_2H_6) = 0.39 \pm 0.02$ at 298 K, independent of pressure. We find that $\Phi(C_2H_6)$ decreases from 0.45 at 12.6 Torr and 298 K or 0.39 at 12.6 Torr and 263 K to a limiting high pressure value of about 0.33 at both temperatures. Thus there are pressure-dependent and pressure-independent processes leading to C_2H_6 formation. Presumably the pressure-independent path comes from predissociation of the initially formed excited singlet states, whereas the pressure-dependent term may come from cross-over to high vibrational levels of the ground singlet state, which can then either dissociate or be pressure quenched. The mechanism could be

$$P + h\nu \longrightarrow {}^1P_n \tag{7}$$

$${}^1P_n \longrightarrow C_2H_6 + CO \tag{8a}$$

$$^1P_n \longrightarrow P_n \tag{8b}$$

$$P_n \longrightarrow C_2H_6 + CO \tag{9}$$

$$P_n + M \longrightarrow P + M \tag{10}$$

where ^1P_n represents high vibrational levels of the excited singlet state and P_n represents high vibrational levels of the ground singlet state. For a given pressure, the results in Table 5 indicate that the relative importance of reaction (9) compared with reaction (10) is lower at the lower temperature, as would be expected for molecules with less internal energy.

The results obtained here for the quenching characteristics of Φ(rad) or $\Phi(C_2H_5)$ are very different from those obtained for $\Phi(C_2H_5)$ from the work of Shepson and Heicklen [51], as can be seen in Table 1. At some wavelengths, they found non-linear Stern–Volmer quenching which they interpreted as quenching from two states, whereas we never found evidence for non-linear Stern–Volmer quenching plots. Even at 254 and 302 nm, where they did find linear Stern–Volmer quenching, our half-quenching pressures differ significantly. The reason for these discrepancies is not known. However, at 312 and 334 nm, where they found two-state quenching, our single quenching half-pressure agrees with their larger value.

With the new data reported here, a straightforward mechanism for Φ(rad) can be proposed:

$$^1P_n \longrightarrow {}^3P_n \tag{8c}$$

$$^3P_n \longrightarrow C_2H_5 + HCO \tag{4}$$

$$^3P_n + M \longrightarrow {}^3P_0 + M \tag{5}$$

where ^3P_n and $^3P_0$ are vibrationally excited triplet C_2H_5CHO and vibrationally cold triplet C_2H_5CHO respectively. In addition, at 334 nm, which is the lowest energy used, the low pressure value for $\Phi(C_2H_5)$ does not approach 1.0, so that some of the initially formed triplet C_2H_5CHO molecules do not have enough energy to dissociate. Thus we include an additional reaction at this wavelength:

$$^1P_n \longrightarrow {}^3P_0 \tag{8d}$$

Earlier work [52] indicates that primary process (1c) or other primary processes are very small (quantum yield, 0.01 or less) at all wavelengths. Thus we ignore these possibilities. Then the mechanism leads to the rate law

$$\Phi(C_2H_5)^{-1} = \frac{k_8}{k_{8c}}\left(1 + \frac{k_5[M]}{k_4}\right) = \frac{1 + \beta_1}{\Phi(\text{rad})} \tag{IV}$$

The Stern–Volmer plots based on eqn. (IV) are shown in Figs. 2 - 8. The intercepts and slopes are listed in Table 4. The intercepts give k_8/k_{8c}. These are close to 1.0 at all wavelengths except at 254 and 334 nm where they are

TABLE 7

Quantum yield for $\Phi(C_2H_5)$ in air at 760 Torr and 298 K

λ (nm)	$\phi(C_2H_5)$
334	0.15
325	0.26
313	0.50
302	0.85
294	0.89

TABLE 8

Data for evaluating atmospheric photodissociation rate coefficients for C_2H_5CHO at 298 K

λ (nm)	σ[a] (cm^2 $molecule^{-1}$)	I_0[b] (photons cm^{-2} s^{-1})	
		$\chi = 30°$	$\chi = 58.18°$
335.0 - 340.0	1.38×10^{-21}	1.119×10^{15}	1.081×10^{15}
330.0 - 335.0	4.83×10^{-21}	1.039×10^{15}	9.883×10^{14}
325.0 - 330.0	8.80×10^{-21}	1.075×10^{15}	9.928×10^{14}
320.0 - 325.0	1.27×10^{-20}	8.309×10^{14}	7.289×10^{14}
315.0 - 320.0	2.03×10^{-20}	6.104×10^{14}	4.847×10^{14}
310.0 - 315.0	3.44×10^{-20}	4.154×10^{14}	2.803×10^{14}
307.7 - 310.0	3.69×10^{-20}	2.327×10^{14}	1.088×10^{14}
303.0 - 307.7	4.07×10^{-20}	7.330×10^{13}	1.771×10^{13}
298.5 - 303.0	5.11×10^{-20}	9.368×10^{12}	7.001×10^{11}
294.1 - 298.5	5.34×10^{-20}	4.315×10^{11}	4.273×10^{9}
289.9 - 294.1	5.93×10^{-20}	2.566×10^{9}	8.83×10^{5}

[a]From McMillan as reported by Calvert and Pitts [52].
[b]Incident intensities from Wuebbles [56].

larger because of the importance of reactions (8a) and (8b) at 254 nm and reaction (8d) at 334 nm. The ratios of the intercepts to the slopes give the k_4/k_5, and these values are listed in Table 1; they increase with increasing radiant energy and temperature, as expected, since the rate of reaction (4) should increase with increasing energy.

Borkowski and Ausloos [46] found the room temperature fluorescence yields of C_2H_5CHO to be almost unaffected by pressure. This is consistent with our mechanism, which indicates that ^1P_n undergoes no pressure quenching. However, they found that the yield of $^3P_0$, as measured by the sensitization of biacetyl phosphorescence, increased by a factor of 3 - 4 as the C_2H_5CHO pressure was increased from 25 to 100 Torr at 313 nm. This is consistent with our findings for the pressure quenching of the radical yield. In contrast, they found that there was only a 10% - 20% increase in $^3P_0$ at 334 nm for a C_2H_5CHO pressure increase from 21 to 108 Torr. Thus most of

the $^3P_0$ formation at 334 nm must come from a pressure-independent process (reaction (8d)), which is consistent with our findings.

4.1. Atmospheric implications

One goal of this work was to calculate the photodissociation rate coefficient for radical production under atmospheric conditions. This rate coefficient k_{rad} is given by

$$k_{rad} = \int I_0 \sigma \Phi(\text{rad}) d\lambda \qquad \text{(V)}$$

where I_0 is the incident photon flux at each wavelength λ, and σ is the absorption cross section at each wavelength. Values for $\Phi(C_2H_5)$ at atmospheric pressure at each wavelength examined in this study are listed in Table 7.

Values of σ and I_0 at two solar zenith angles χ over various wavelength intervals are given in Table 8. With these data k_{rad} is computed to be 2.4×10^{-5} s^{-1} at $\chi = 30°$ and 1.6×10^{-5} s^{-1} at $\chi = 58.18°$.

Acknowledgment

This work was supported by the Atmospheric Sciences Section of the National Science Foundation under Grant ATM-8211603 for which we are grateful.

References

1 A. C. Lloyd, *Nat. Bur. Stand. (U.S.), Spec. Publ., 557* (1979) 27.
2 J. E. Carruthers and R. G. W. Norrish, *J. Chem. Soc.*, (1936) 1036.
3 E. C. A. Horner and D. W. G. Style, *Trans. Faraday Soc., 50* (1954) 1197.
4 T. C. Purcell and I. R. Cohen, *Environ. Sci. Technol., 1* (1967) 845.
5 J. J. Bufalini and K. L. Brubaker, in C. Tuesday (ed.), *Chemical Reactions in Urban Atmospheres*, Elsevier, New York, 1971, p. 225.
6 R. G. Miller and E. K. C. Lee, *Chem. Phys. Lett., 27* (1974) 475.
7 P. L. Houston and C. B. Moore, *J. Chem. Phys., 65* (1976) 757.
8 T. L. Osif, *Ph.D. Dissertation*, The Pennsylvania State University, 1976.
9 P. Avouris, W. M. Gelbart and M. A. El-Sayed, *Chem. Rev., 77* (1977) 793.
10 F. Su, A. Horowitz and J. G. Calvert, *Int. J. Chem. Kinet., 10* (1978) 1099.
11 J. R. Sodeau and E. K. C. Lee, *Chem. Phys. Lett., 57* (1978) 71.
12 A. Horowitz and J. Calvert, *Int. J. Chem. Kinet., 10* (1978) 713.
13 A. Horowitz and J. Calvert, *Int. J. Chem. Kinet., 10* (1978) 805.
14 J. H. Clark, C. B. Moore and N. S. Nogar, *J. Chem. Phys., 68* (1978) 1264.
15 R. S. Lewis and E. K. C. Lee, *J. Phys. Chem., 82* (1978) 249.
16 G. K. Moortgat, F. Slemr, W. Seiler and P. Warneck, *Chem. Phys. Lett., 54* (1978) 444.
17 F. Su, J. G. Calvert and J. H. Shaw, *J. Phys. Chem., 83* (1979) 3185.
18 F. Su, J. G. Calvert, J. H. Shaw, H. Niki, P. D. Maker, C. M. Savage and L. D. Breitenbach, *Chem. Phys. Lett., 65* (1979) 221.
19 G. K. Moortgat and P. Warneck, *J. Chem. Phys., 70* (1979) 3639.
20 B. M. Morrison, Jr., and J. Heicklen, *J. Photochem., 11* (1979) 183.

21 B. M. Morrison, Jr., and J. Heicklen, *J. Photochem., 13* (1980) 189.
22 E. K. C. Lee and R. S. Lewis, *Adv. Photochem., 12* (1980) 1.
23 B. M. Morrison, Jr., and J. Heicklen, *J. Photochem., 15* (1981) 131.
24 C. B. Moore, *Ann. Rev. Phys. Chem., 34* (1983) 525.
25 E. J. Bowen and E. L. Tietz, *J. Chem. Soc.*, (1930) 234.
26 J. Mignolet, *Bull. Soc. R. Sci. Liege, 10* (1941) 343.
27 C. A. McDowell and L. K. Sharples, *Can. J. Chem., 36* (1958) 251.
28 C. A. McDowell and L. K. Sharples, *Can. J. Chem., 36* (1958) 268.
29 J. G. Calvert and P. L. Hanst, *Can. J. Chem., 37* (1959) 1671.
30 C. A. McDowell and S. Sifoniades, *Can. J. Chem., 41* (1963) 300.
31 C. S. Parmenter and W. A. Noyes, Jr., *J. Am. Chem. Soc., 85* (1963) 416.
32 H. S. Johnston and J. Heicklen, *J. Am. Chem. Soc., 86* (1964) 4254.
33 A. S. Archer, R. B. Cundall and T. F. Palmer, *Proc. R. Soc. London, Ser. A, 334* (1973) 411.
34 J. Weaver, J. Meagher, R. Shortridge and J. Heicklen, *J. Photochem., 4* (1975) 341.
35 N. A. Clinton, R. A. Kenley and T. G. Traylor, *J. Am. Chem. Soc., 97* (1975) 3746.
36 J. Weaver, J. Meagher and J. Heicklen, *J. Photochem., 6* (1976) 111.
37 R. J. Gill and G. H. Atkinson, *Chem. Phys. Lett., 64* (1979) 426.
38 H. Meyrahn, G. K. Moortgat and P. Warneck, *J. Photochem., 17* (1981) 138.
39 R. J. Gill, W. D. Johnson and G. H. Atkinson, *Chem. Phys., 58* (1981) 29.
40 A. Horowitz and J. G. Calvert, *J. Phys. Chem., 86* (1982) 3094.
41 A. Horowitz and J. G. Calvert, *J. Phys. Chem., 86* (1982) 3105.
42 R. Simonaitis and J. Heicklen, *J. Photochem., 23* (1983) 299.
43 G. K. Moortgat, W. Seiler and P. Warneck, *J. Chem. Phys., 78* (1983) 1185.
44 F. E. Blacet and J. N. Pitts, Jr., *J. Am. Chem. Soc., 74* (1952) 3382.
45 C. A. McDowell and L. K. Sharples, *Can. J. Chem., 16* (1958) 258.
46 R. P. Borkowski and P. Ausloos, *J. Am. Chem. Soc., 84* (1962) 4044.
47 A. P. Altshuller, I. R. Cohen and T. C. Purcell, *Can. J. Chem., 44* (1966) 2973.
48 S. L. Kopczynski, A. P. Altshuller and F. D. Sutterfield, *Environ. Sci. Technol., 8* (1974) 909.
49 D. A. Hansen and E. K. C. Lee, *J. Chem. Phys., 63* (1975) 3272.
50 P. Shepson and J. Heicklen, *J. Photochem., 18* (1982) 169.
51 P. Shepson and J. Heicklen, *J. Photochem., 19* (1982) 215.
52 J. G. Calvert and J. N. Pitts, Jr., *Photochemistry*, Wiley, New York, 1966.
53 NASA Panel for Data Evaluation, Chemical Kinetics and Photochemical Data for Use in Stratospheric Modeling, *Jet Propulsion Lab. Publ., 83 - 62*, 1983, p. 136.
54 H. Okabe, *J. Chem. Phys., 66* (1973) 2058.
55 R. Renaud and L. C. Leitch, *Can. J. Chem., 32* (1954) 549.
56 D. Wuebbles, personal communication, 1981.